DOI: 10.1002/ejic.201000580

Uniform Fe_3O_4 Octahedra with Tunable Edge Length – Synthesis by a Facile Polyol Route and Magnetic Properties

Lijun Zhao*[a] and LianFeng Duan[a]

Keywords: Iron / Nanoparticles / Polyol synthesis / Tunable size / Magnetic properties

A straightforward and effective polyol route for the controllable synthesis of high-quality magnetite (Fe_3O_4) octahedra with uniform edge length in ethylene glycol (EG) solution is presented. Fe_3O_4 octahedra with edge length in the range 70–1000 nm were selectively synthesized in high yield. The surfaces of octahedral Fe_3O_4 crystals correspond to (111) planes. Formation of Fe_3O_4 octahedra was attributed to the preferential adsorption of OH^- ions onto the (111) planes of Fe_3O_4 nuclei, which inhibits the growth rate along the <111> direction. The release rate of Fe^{2+} ions in the synthesis can be rationally manipulated by varying the dose of $N_2H_4{\cdot}H_2O$. Control of the nucleation and growth rate by $N_2H_4{\cdot}H_2O$ provides a facile and effective route to harvest Fe_3O_4 octahedra with different dimensions. The magnetic analysis shows that Fe_3O_4 octahedra with sharp tips possess attractive magnetic properties.

Introduction

Magnetic particles of iron oxide, Fe_3O_4, have been investigated extensively as functional materials for ferrofluids, high-density information storage, gas sensors, magnetic resonance imaging, controlled drug release of therapeutic agents, labeling and sorting of cells, and immunomagnetic separation.[1–3] Furthermore, Fe_3O_4 particles are widely studied due to their potential applications in biology and medicine such as enzyme and protein immobilization, magnetic cell separation and purification, magnetic resonance imaging, RNA and DNA purification, and magnetically controlled transport of anticancer drugs.[4–9] Shape and size are the main factors that determine the chemical and physical properties of crystals, which may serve as bases for the development of new investigative fields. Although the methodology for the preparation of octahedra is mature, it remains a challenge to control the edge length of octahedra in a narrow distribution and over a wide adjustable range. Until now, there has been little attention paid to the synthesis of Fe_3O_4 octahedra with tunable edge length. It is therefore of necessity and significance to perform a relatively comprehensive study on this subject with special focus on the variations in the magnetic properties of the products with their size and shape. Understanding the effect of size and shape on properties is important, as Fe_3O_4 has potential applications in biological fields, where particles with different sizes may have differential affinity for special cells.

Much effort has been devoted to synthesizing various Fe_3O_4 crystals with different shapes.[10–17] Polyhedral particles, as a special type of faceted materials, have been demonstrated to possess unique properties associated with their facets, edges, and even corners.[18–21] Alkali metals can move easily on the Fe_3O_4 (111) surface, consequently the catalytic ability of the defined alkali metal can be enhanced.[22] Despite some progress in the synthesis of micro/sub-microscale and nanoscale Fe_3O_4 octahedra,[23,24] the synthesis of Fe_3O_4 octahedra having tunable size, sharp edge length distribution, and uniform shape have met with very limited success. Moreover, it is difficult to directly and systematically tailor the dimension of octahedral Fe_3O_4 crystals over a wide range by using the previously reported methods. Surfactants are usually used to control the size and shape of crystals, but in this contribution, we provide a strategy to fabricate Fe_3O_4 octahedra with controllable lateral size and shape independent of surfactants, temperature, and time of reaction. By introducing $N_2H_4{\cdot}H_2O$ into the reaction medium, the final edge length can be readily controlled, and consequently the dimensions of the Fe_3O_4 octahedra can be systematically tailored over a wide range in a straightforward way. Interestingly, it is not the edge length but the vertex angle of the Fe_3O_4 octahedra that has the greatest effect on the magnetic properties.

Results and Discussion

XRD patterns of Fe_3O_4 octahedra with different edge lengths are shown in Figure 1. All the diffraction peaks can be indexed to a pure face-centered cubic phase [fcc, space group *Fd*3*m* (No. 227)] of magnetite. Furthermore, the samples are black, which confirms that magnetite (black) was prepared rather than maghemite (brown). The diffraction

[a] Key Laboratory of Automobile Materials (Jilin University), Ministry of Education and School of Materials Science and Engineering, Jilin University,
Changchun 130022, China
Fax: +86-431-85095876
E-mail: lijunzhao@jlu.edu.cn

peaks in the XRD patterns can be indexed to the face-centered cubic structure of magnetite according to JCPDS card no. 19–0629 and have similar intensity and position for all samples. , Likewise, there are few differences among the samples in the full width at half maximum (FWHM) value for the most intense peak (311).This peak may be due to the existence of strain in the Fe_3O_4 octahedra. The crystal structure does not change with the dose of $N_2H_4{\cdot}H_2O$; however, once the dose is more than 2 mL, we cannot obtain Fe_3O_4 octahedra, although the samples retain the pure fcc structure of magnetite.

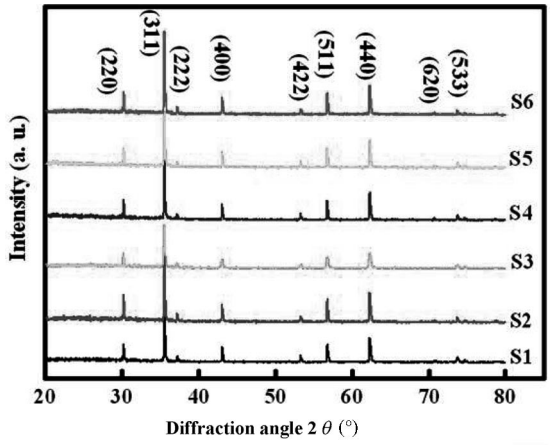

Figure 1. XRD patterns of S1 to S6.

By SEM investigation, we can observe visually the effect of the dose of $N_2H_4{\cdot}H_2O$ on the edge length and vertex angles of Fe_3O_4 octahedra. Figure 2 shows the SEM images

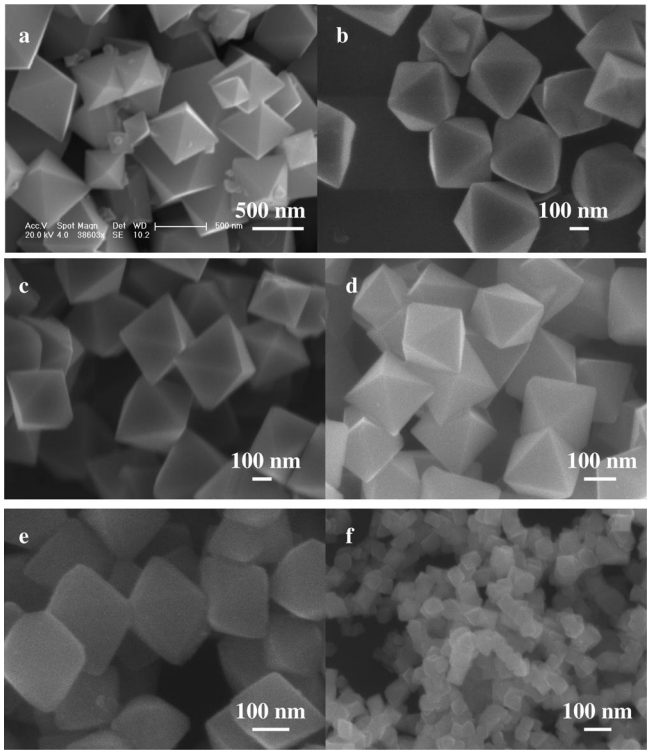

Figure 2. SEM images of (a) S1, (b) S2, (c) S3, (d) S4, (e) S5, and (f) S6.

of S1 to S6. From the SEM images, we can sum up three conclusions.

(1) The edge lengths of Fe_3O_4 octahedra decrease with an increase in the dose of $N_2H_4{\cdot}H_2O$. Regulating the dose of $N_2H_4{\cdot}H_2O$ provides a broad range of lateral size distribution (70 to 1000 nm). The edge lengths of S1 to S6 are shown in Table 1.

Table 1. Dose of $N_2H_4{\cdot}H_2O$ for the synthesis of samples with tunable edge length.

Samples	S1	S2	S3	S4	S5	S6
$N_2H_4{\cdot}H_2O$ (mL)	0.00	1.00	1.25	1.50	1.75	2.00
Edge length (nm)	200–1000	400	300	200	160	70

(2) The edge length of Fe_3O_4 octahedra prepared with the aid of $N_2H_4{\cdot}H_2O$ are uniform.

(3) The increasing sequence for a vertex angle of one facet of Fe_3O_4 octahedra is S3, S4, S2, S1, S5, and S6.

Here, we should consider the two key factors in deciding the morphologies and edge length of Fe_3O_4 crystals. In fact, OH^- ions and $N_2H_4{\cdot}H_2O$ play the crucial roles in determining separately the morphologies and edge length of Fe_3O_4 crystals.

The Fe_3O_4 octahedra are enclosed by (111) planes, as shown in Figure 3b, which have the lowest surface energy for the face-centered cubic crystal structure. The anisotropy of the crystal structure, or the crystal surface reactivity, is identified as the main driving force of the growth of anisotropic structure. The influence of chemical potential on shape evolution has been elucidated by Peng et al.[25,26] In the case of crystal growth, it is beneficial to have a higher chemical potential, which is mainly determined by the concentration of NaOH. Fe_3O_4 octahedra with high quality and crystallization will be obtained in concentrated NaOH solutions, because both high concentration of OH^- ions and high chemical potential in solution favor the growth of octahedral structures over other possible crystal forms. From the point of view of kinetics of crystal growth, if the crystal adsorbs hydroxy groups on some areas of its surface, the growth rate of the crystal in certain directions will be confined. Therefore, the concentration of NaOH can modify the growth kinetics of the crystal, which leads to the anisotropic growth of the crystals. In other words, the concentrated NaOH solution is in favor of the quick growth of Fe_3O_4 octahedra.

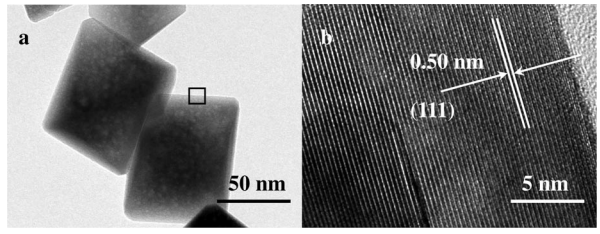

Figure 3. (a) TEM and (b) HRTEM images of S6.

How can the effect of $N_2H_4{\cdot}H_2O$ on the lateral size of Fe_3O_4 octahedra be explained?

Firstly, the lateral sizes of Fe_3O_4 octahedra depend strongly on the Ostwald ripening process. Therefore, the key to size control lies in tuning the competition between nucleation and growth. When the growth ratio of seeds is larger than the nucleation ratio, the size of the Fe_3O_4 octahedra will be smaller. The preparation of Fe_3O_4 probably involves the following chemical reactions [Equations (1), (2) and (3)]:

$$Fe^{2+}+2OH^- \rightarrow Fe(OH)_2 \quad (1)$$

$$3Fe(OH)_2 + 1/2O_2 \rightarrow Fe(OH)_2 + 2FeOOH + H_2O \quad (2)$$

$$Fe(OH)_2 + 2FeOOH \rightarrow Fe_3O_4 + 2H_2O \quad (3)$$

Thus, it is concluded that in the synthesis with ferrous ions alone, Fe_3O_4 is formed because of the dehydration reaction of ferrous hydroxide and ferric oxide–hydroxide, as represented by Equation (3), in which the latter compound is produced by the partial oxidation of ferrous hydroxide by O_2 dissolved in the reacting system, according to Equation (2). The formation of $Fe(OH)_2$ would be the first process of the synthesis. A change in the experimental parameters in Equation (1) can therefore control the size of the Fe_3O_4 octahedra. $N_2H_4{\cdot}H_2O$ can kinetically manipulate Equations (1) and (2), and this in turn affects the initial Fe_3O_4 nucleation process, which is one of determining factors for the edge length of the final products. A slow nucleation process and quick growth makes for Fe_3O_4 octahedra with a narrow edge length size distribution. With the increasing addition of $N_2H_4{\cdot}H_2O$, the nucleation process will be slower, because of the complexion of Fe^{2+} ions with $N_2H_4{\cdot}H_2O$. Concurrently, the dissolved O_2 in the reacting system increases with higher doses of $N_2H_4{\cdot}H_2O$ in ethylene glycol (EG) solution. Thus, slower nucleation and quicker growth occur upon the addition of $N_2H_4{\cdot}H_2O$, which facilitates the formation of Fe_3O_4 octahedra with a shorter edge length. Furthermore, the increase in ionic strength due to more $N_2H_4{\cdot}H_2O$ in the NaOH solution can affect the sizes of the particles as well. An increase in the ionic strength of

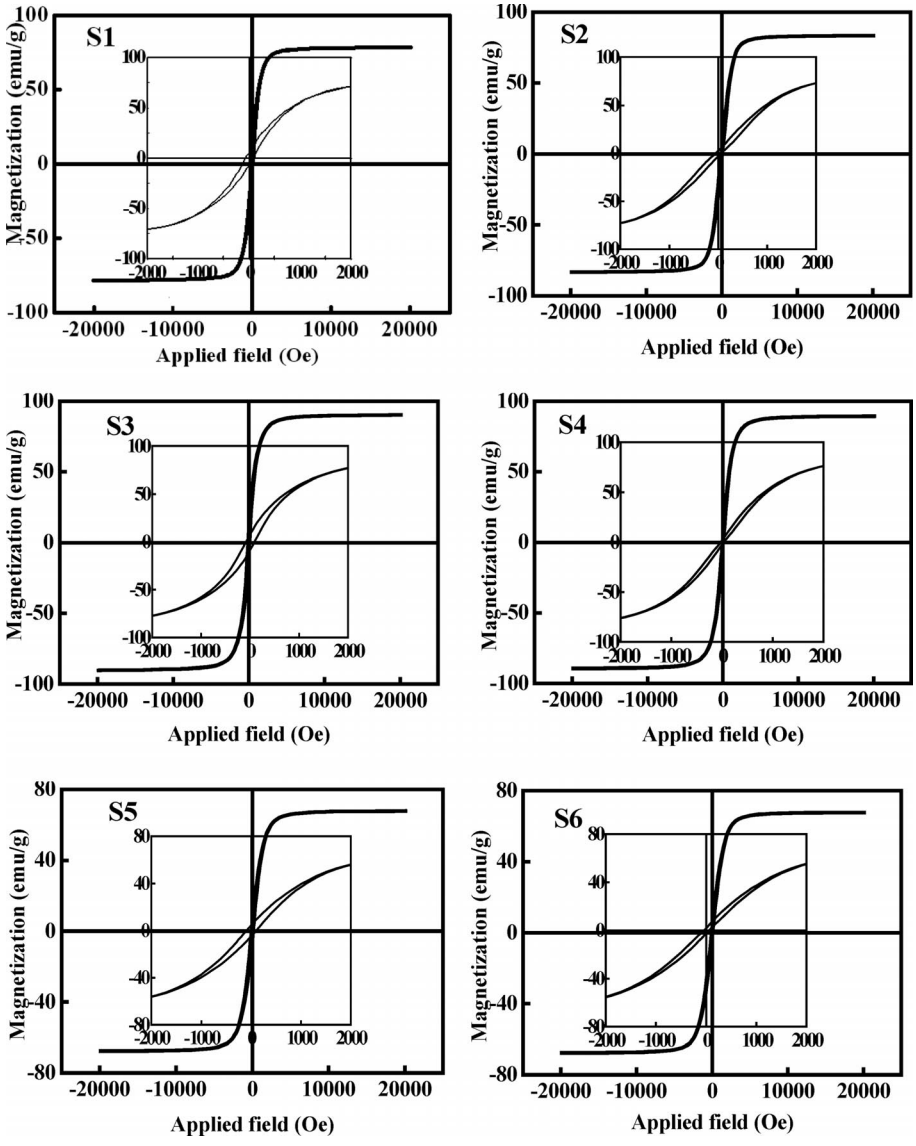

Figure 4. Magnetization curve measured at room temperature for S1 to S6.

the solution will slow the growth and nucleation ratio at the same time on the basis of the decrease in the activity of precursor ions; hence, Fe_3O_4 octahedra with shorter edge length can be obtained.

Secondly, increasing the dose of $N_2H_4{\cdot}H_2O$ leads to an enhancement of solution alkalinity in the reaction system, which causes the quick generation of Fe_3O_4 and hence produces small Fe_3O_4 octahedra. On the contrary, when the generation of Fe_3O_4 becomes slow with a decrease in solution alkalinity, large Fe_3O_4 octahedra are produced. The vertex angle does not simply vary with the amount of $N_2H_4{\cdot}H_2O$ or edge length, because it may be influenced by the reduction rate and viscosity of the reaction system. With increasing dose of $N_2H_4{\cdot}H_2O$, the reduction rate is increased and the viscosity of the reaction system is decreased. By considering the joint function of reduction rate and viscosity of the reaction system, Fe_3O_4 octahedra with different vertex angles were obtained.

Further insight into the morphology and structure of Fe_3O_4 nanooctahedra were gained by using TEM and HRTEM. Figure 3a shows the TEM image of S6. HRTEM was performed in the region of nanooctahedron, as labeled in Figure 3a, and the micrograph is shown in Figure 3b. Lattice fringes of the Fe_3O_4 nanocrystal can be seen clearly. The interplanar spacing was measured to be 0.45 nm, corresponding to the (111) planar spacing of cubic Fe_3O_4. The HRTEM image exhibits well-defined lattices that go straight through the entire particle without stacking faults or twins, indicating that as-prepared S6 is composed of single crystals. On the basis of the HRTEM image, it is suggested that the Fe_3O_4 nanocrystals are enclosed by (111) planes, that is, octahedral shape.

Magnetization measurements were performed to investigate the dependence of the magnetic properties of Fe_3O_4 octahedra upon their lateral sizes. Figure 4 shows the hysteresis loops of S1 to S6 measured in fields between ± 2 T at room temperature.

Moreover, in order to explore the relationship between vertex angles of isosceles-triangular crystal planes for S1 to S6 and their magnetic properties, we measured the vertex angle selected from SEM and TEM images of S1 to S6. Figure 5 shows the schematic illustration for the vertex angles of the samples.

The magnetic parameters and vertex angles obtained from Figures 4 and 5 are listed in Table 2. An orbiting electron in an atom will have a magnetic dipole moment; hence, we hypothesize that Fe_3O_4 octahedra with sharp tips may show strong dipolar interactions between electrons. Dipolar interactions can suppress thermal fluctuations and the alignment of spins with an applied field, and thus cause an increase in saturation magnetization. The saturation magnetizations of S5 and S6 show an abrupt decrease, which may be attributed to the slightly rounded apexes of S5 and S6, that is, a weak dipolar interaction. The coercivity is defined as a measure of the magnetic field strength that is required to achieve changes of magnetization direction in a material. Many factors play important roles in determining the coercivity. The observed coercivity is a combination of many anisotropy mechanisms, such as magnetocrystalline anisotropy, surface anisotropy, and interparticle interactions. Strong dipolar interactions block the rotation of spins to align with the field, which results in an increase in coercivity. It was reported that for small magnetite particles magnetocrystalline anisotropy is the dominant form of anisotropy.[27] The above-mentioned reasons may be responsible for the different values of coercivity and remnant magnetization.

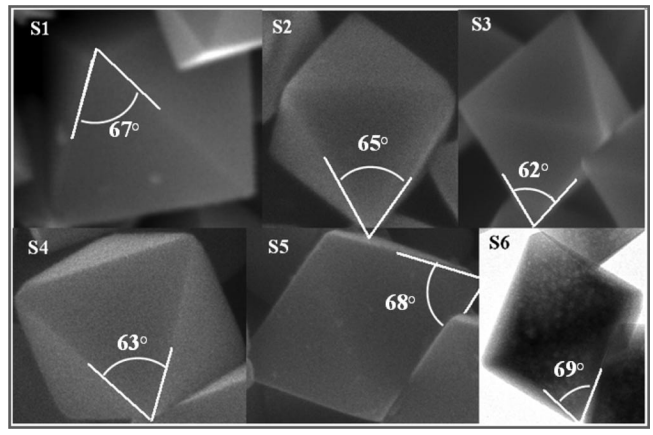

Figure 5. Schematic illustration of the vertex angle of isosceles-triangular crystal planes for S1 to S6.

Table 2. Magnetic parameters of Fe_3O_4 octahedra with different edge lengths and vertex angles tested by SQUID at room temperature.

Sample	S1	S2	S3	S4	S5	S6
Vertex angles	67°	65°	62°	63°	68°	69°
Edge length (nm)	200–1000	400	300	200	160	70
M_s (emu/g)	79	83	91	89	68	68
M_r (emu/g)	6.5	3	8.4	2.3	4.6	2.2
H_c (Oe)	80	55	90	35	98	56

Conclusions

Large-scale and uniform Fe_3O_4 octahedra with edge lengths of 70 to 1000 nm were synthesized by manipulating the dosee of $N_2H_4{\cdot}H_2O$ in EG solution. $N_2H_4{\cdot}H_2O$ kinetically manipulates the nucleation and growth process, allowing for the preparation of Fe_3O_4 octahedra with different dimensions. The edge length of Fe_3O_4 octahedra were found to decrease with an increase in the dose of $N_2H_4{\cdot}H_2O$. The increasing sequence for the vertex angle of one facet of the Fe_3O_4 octahedra is S3, S4, S2, S1, S5, and S6. Magnetic analysis shows that the decisive factor for the magnetic properties of Fe_3O_4 is not the edge length, but instead the vertex angles of Fe_3O_4 octahedra.

Experimental Section

All chemicals were of analytical grade and were used without further purification. $FeSO_4$ solution (2 mL, 0.5 mol L^{-1}) was dissolved in EG (20 mL) to form a homogeneous solution. Hydrazine mono-

hydrate, $N_2H_4{\cdot}H_2O$ (55 vol.-%), was added dropwise to the solution at room temperature, and the mixture was stirred vigorously for 20 min. NaOH solution (5 mol L^{-1}) was then quickly added to the solution at room temperature, followed by intensive stirring (30 min) in air. The mixture was transferred into a 30 mL stainless steel autoclave lined with Teflon, sealed, and maintained at 200 °C for 24 h. After completion of the reaction, the black residue was collected by magnetic separation and washed several times with water and ethanol. The final black products were dried in a vacuum oven at 40 °C for 6 h. Detailed experimental parameters and corresponding edge lengths of Fe_3O_4 octahedra are listed in Table 1 (from S1 to S6).

The phases were identified by means of X-ray diffraction (XRD) with a Rigaku D/max 2500pc X-ray diffractometer with Cu-K_α radiation (λ = 1.54156 Å) at a scan rate of 0.04°S^{-1}. The morphologies were characterized by a JEOL JSM-6700F field-emission scanning electron microscope (FESEM) operated at an acceleration voltage of 8.0 kV. Transmission electron microscopy (TEM), high-resolution TEM (HRTEM) observations, and selected area electron diffraction (SAED) patterns were obtained by using a JEOL 2100F instrument with an emission voltage of 200 kV. Magnetic measurements were carried out with a Quantum Design super conducting quantum interference device (SQUID) magnetometer (LakeShore 7307).

Acknowledgments

This work was supported by the Natural Science Foundation of Jilin Province (20101542) and the Basic Research Expenses for the Special Funds of Jilin University.

[1] H. Wei, E. Wang, *Anal. Chem.* **2008**, *80*, 2250–2254.
[2] G. Lv, F. He, X. Wang, F. Gao, G. Zhang, T. Wang, H. Jiang, C. Wu, D. Guo, X. Li, B. Chen, Z. Gu, *Langmuir* **2008**, *24*, 2151–2156.
[3] S. W. Cao, Y. J. Zhu, M. Y. Ma, L. Li, L. Zhang, *J. Phys. Chem. C* **2008**, *112*, 1851–1856.
[4] A. K. Gupta, M. Gupta, *Biomaterials* **2005**, *26*, 3995–4021.
[5] C. J. Xu, K. M. Xu, H. W. Gu, R. K. Zheng, H. Liu, X. X. Zhang, Z. H. Guo, B. Xu, *J. Am. Chem. Soc.* **2004**, *126*, 9938–9939.
[6] H. W. Gu, K. M. Xu, C. J. Xu, B. Xu, *Chem. Commun.* **2006**, 941–949.
[7] Z, M. Saiyed, C. Bochiwal, H. Gorasia, S. D. Telang, C. N. Ramchand, *Anal. Biochem.* **2006**, *356*, 306–308.
[8] F. Q. Hu, L. Wei, Z. Zhou, Y. L. Ran, Z. Li, M. Y. Gao, *Adv. Mater.* **2006**, *18*, 2553–2556.
[9] J. Xie, C. J. Xu, Z. C. Xu, Y. L. Hou, K. L. Young, S. X. Wang, N. Pourmond, S. H. Sun, *Chem. Mater.* **2006**, *18*, 5401–5403.
[10] H. Deng, X. L. Li, Q. Peng, X. Wang, J. P. Chen, Y. D. Li, *Angew. Chem. Int. Ed.* **2005**, *44*, 2782–2785.
[11] X. M. Liu, S. Y. Fu, L. P. Zhu, *J. Solid State Chem.* **2007**, *180*, 461–466.
[12] D. E. Zhang, X. J. Zhang, X. M. Ni, J. M. Song, H. G. Zheng, *J. Magn. Magn. Mater.* **2006**, *305*, 68–70.
[13] H. Wang, Q. W. Chen, Y. B. Sun, M. S. Wang, L. X. Sun, W. S. Yan, *Langmuir* **2010**, *26*, 5957–5962.
[14] Y. L. Chueh, M. W. Lai, J. Q. Liang, L. J. Chou, Z. L. Wang, *Adv. Funct. Mater.* **2006**, *16*, 2243–2251.
[15] Z. H. Ai, K. J. Deng, Q. F. Wan, L. Z. Zhang, S. H. Lee, *J. Phys. Chem. C* **2010**, *114*, 6237–6242.
[16] D. B. Yu, X. Q. Sun, J. W. Zou, Z. R. Wang, F. Wang, K. Tang, *J. Phys. Chem. B* **2006**, *110*, 21667–21671.
[17] N. Zhao, W. Ma, Z. M. Cui, W. G. Song, C. L. Xu, M. Y. Gao, *ACS Nano* **2009**, *3*, 1775–1780.
[18] N. Tian, Z. Y. Zhou, S. G. Sun, Y. Ding, Z. L. Wang, *Science* **2007**, *316*, 732–735.
[19] J. G. Zhang, Y. Gao, R. A. Alvarez-Puebla, J. M. Buriak, H. Fenniri, *Adv. Mater.* **2006**, *18*, 3233–3237.
[20] Y. H. Zheng, Y. Cheng, Y. S. Wang, F. Bao, L. H. Zhou, X. F. Wei, Y. Y. Zhang, Q. Zheng, *J. Phys. Chem. B* **2006**, *110*, 3093–3097.
[21] F. Kim, S. Connor, H. Song, T. Kuykendall, P. D. Yang, *Angew. Chem. Int. Ed.* **2004**, *43*, 3673–3677.
[22] T. Yang, X. D. Wen, Y. W. Li, J. G. Wang, H. J. Jiao, *Surf. Sci.* **2009**, *603*, 78–83.
[23] L. J. Zhao, H. J. Zhang, Y. Xing, S. Y. Song, S. Y. Yu, W. D. Shi, X. M. Guo, J. H. Yang, Y. Q. Lei, F. Cao, *Chem. Mater.* **2008**, *20*, 198–204.
[24] L. H. Zhang, J. J. Wu, H. B. Liao, Y. L. Hou, S. Gao, *Chem. Commun.* **2009**, 4378–4380.
[25] A. Z. Peng, X. G. Peng, *J. Am. Chem. Soc.* **2001**, *123*, 1389–1395.
[26] A. Z. Peng, X. G. Peng, *J. Am. Chem. Soc.* **2002**, *124*, 3343–3247.
[27] B. D. Cullity, *Introduction to Magnetic Materials*, Addison-Wesley Publishing, Reading, MA, **1972**, pp. 410–421.

Received: May 25, 2010
Published Online: November 22, 2010

